Resonant Modes in a Maser Interferometer

By A. G. FOX and TINGYE LI

(Manuscript received October 20, 1960)

A theoretical investigation has been undertaken to study diffraction of electromagnetic waves in Fabry-Perot interferometers when they are used as resonators in optical masers. An electronic digital computer was programmed to compute the electromagnetic field across the mirrors of the interferometer where an initially launched wave is reflected back and forth between the mirrors.

It was found that after many reflections a state is reached in which the relative field distribution does not vary from transit to transit and the amplitude of the field decays at an exponential rate. This steady-state field distribution is regarded as a normal mode of the interferometer. Many such normal modes are possible depending upon the initial wave distribution. The lowest-order mode, which has the lowest diffraction loss, has a high intensity at the middle of the mirror and rather low intensities at the edges. Therefore, the diffraction loss is much lower than would be predicted for a uniform plane wave. Curves for field distribution and diffraction loss are given for different mirror geometries and different modes.

Since each mode has a characteristic loss and phase shift per transit, a uniform plane wave which can be resolved into many modes cannot, properly speaking, be resonated in an interferometer. In the usual optical interferometers, the resolution is too poor to resolve the individual mode resonances and the uniform plane wave distribution may be maintained approximately. However, in an oscillating maser, the lowest-order mode should dominate if the mirror spacing is correct for resonance.

A confocal spherical system has also been investigated and the losses are shown to be orders of magnitude less than for plane mirrors.

I. INTRODUCTION

Schawlow and Townes[1] have proposed infrared and optical masers using Fabry-Perot interferometers as resonators. Very recently, Mai-

man[2] and Collins et al.[3] have demonstrated experimentally the feasibility of stimulated optical radiation in ruby. In these experiments two parallel faces of the ruby sample were polished and silvered so as to form an interferometer. The radiation due to stimulated emission resonates in the interferometer and emerges from a partially silvered face as a coherent beam of light.

In a maser using an interferometer for a resonator, a wave leaving one mirror and traveling toward the other will be amplified as it travels through the active medium. At the same time it will lose some power due to scattering by inhomogeneities in the medium. When the wave arrives at the second mirror some power will be lost in reflection due to the finite conductivity of the mirror and some power will be lost by radiation around the edges of the mirror. For oscillation to occur, the total loss in power due to density scattering, diffractive spillover and reflection loss must be less than the power gained by travel through the active medium. Thus diffraction loss is expected to be an important factor, both in determining the start-oscillation condition, and in determining the distribution of energy in the interferometer during oscillation.

While it is common practice to regard a Fabry-Perot interferometer as being simultaneously resonant for uniform plane waves traveling parallel to the axis and at certain discrete angles from the axis, this picture is not adequate for the computation of diffraction loss in a maser. It is true that, when the interferometer is operated as a passive instrument with uniform plane waves continuously supplied from an external source, the internal fields may be essentially those of uniform plane waves. In an oscillating maser where power is supplied only from within the interferometer, the recurring loss of power from the edges of a wave due to diffraction causes a marked departure from uniform amplitude and phase across the mirror.

The purpose of our study is to investigate the effects of diffraction on the electromagnetic field in a Fabry-Perot interferometer in free space. The conclusions can be applied equally well to gaseous or solid state masers provided the interferometer is immersed in the active medium, i.e., there are no side-wall discontinuities.

II. FORMULATION OF THE PROBLEM

2.1 *General Formulation*

Our approach is to consider a propagating wave which is reflected back and forth by two parallel plane mirrors, as shown in Fig. 1(a). [This is

equivalent to the case of a transmission medium comprising a series of collinear identical apertures cut into parallel and equally spaced black (perfectly absorbing) partitions of infinite extent, as in Fig. 1(b).] We assume at first an arbitrary initial field distribution at the first mirror and proceed to compute the field produced at the second mirror as a result of the first transit. The newly calculated field distribution is then used to compute the field produced at the first mirror as a result of the second transit. This computation is repeated over and over again for subsequent successive transits. The questions we have in mind are: (a) whether, after many transits, the relative field distribution approaches a steady state; (b) whether, if a steady-state distribution results, there are any other steady-state solutions; and (c) what the losses associated with these solutions would be. While it is by no means obvious that steady-state solutions (corresponding to normal modes) exist for a system which has no side-wall boundaries, it will be shown that such solutions do indeed exist.*

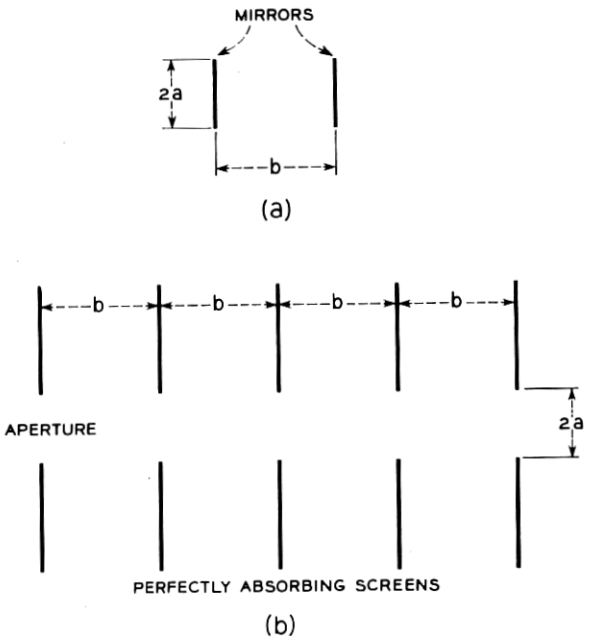

Fig. 1 — The Fabry-Perot interferometer and the transmission medium analog.

* Schawlow and Townes[1] suggested the possibility that resonant modes for a parallel plate interferometer might be similar in form to those for a totally enclosed cavity.

We shall use the scalar formulation of Huygens' principle to compute the electromagnetic field at one of the mirrors in terms of an integral of the field at the other. This is permissible if the dimensions of the mirror are large in terms of wavelength and if the field is very nearly transverse electromagnetic and is uniformly polarized in one direction. Later, we shall show that these assumptions are consistent with the results of our solutions and therefore are justifiable. We shall also show that other polarization configurations can be constructed from the solutions of the scalar problem by linear superposition.

The Fresnel field u_p due to an illuminated aperture A is given by the surface integral[4]

$$u_p = \frac{jk}{4\pi} \int_A u_a \frac{e^{-jkR}}{R} (1 + \cos \theta)\, dS, \tag{1}$$

where u_a is the aperture field, k is the propagation constant of the medium, R is the distance from a point on the aperture to the point of observation and θ is the angle which R makes with the unit normal to the aperture. We now assume that an initial wave of distribution u_p is launched at one of the mirrors of the interferometer and is allowed to be reflected back and forth in the interferometer. After q transits the field at a mirror due to the reflected field at the other is simply given by (1) with u_p replaced by u_{q+1}, which is the field across the mirror under consideration and u_a by u_q, which is the reflected field across the opposite mirror giving rise to u_{q+1}.

It is conceivable that after many transits the distribution of field at the mirrors will undergo negligible change from reflection to reflection and will eventually settle down to a steady state. At this point the fields across the mirrors become identical except for a complex constant; that is,

$$u_q = \left(\frac{1}{\gamma}\right)^q v\,, \tag{2}$$

where v is a distribution function which does not vary from reflection to reflection and γ is a complex constant independent of position coordinates. Substituting (2) in (1) we have the integral equation

$$v = \gamma \int_A Kv\, dS \tag{3}$$

in which the kernel of the integral equation, K, is equal to $(jk/4\pi R) \cdot (1 + \cos \theta) e^{-jkR}$. The distribution function v, which satisfies (3), can

be regarded as a normal mode of the interferometer defined at the mirror surface, and the logarithm of γ, which specifies the attenuation and the phase shift the wave suffers during each transit, can be regarded as the propagation constant associated with the normal mode.

The integral equation (3) can be solved numerically by the method of successive approximations (Ref. 5, p. 421). It is interesting to note that this iterative method of solution is analogous to the physical process of launching an initial distribution of wavefront in the interferometer and letting it bounce back and forth between the mirrors as described in the foregoing paragraphs.

We have studied and obtained numerical solutions for several geometric configurations of the interferometer. These are (a) rectangular plane mirrors, (b) circular plane mirrors and (c) confocal spherical or paraboloidal mirrors.

2.2 *Rectangular Plane Mirrors*

When the mirror separation is very much larger than the mirror dimensions the problem of the rectangular mirrors reduces to a two-dimensional problem of infinite strip mirrors. This is shown in Appendix A. The integral equation for the problem of infinite strip mirrors, when $a^2/b\lambda$ is much less than $(b/a)^2$, is

$$v(x_2) = \gamma \int_{-a}^{a} K(x_2, x_1) v(x_1)\, dx_1 \tag{4}$$

with

$$K(x_2, x_1) = \frac{e^{j(\pi/4)}}{\sqrt{\lambda b}}\, e^{-jk(x_1 - x_2)^2/2b} \tag{4a}$$

The various symbols are defined in Fig. 2 and Appendix A.

Equation (4) is a homogeneous linear integral equation of the second kind. Since the kernel is continuous and symmetric [$K(x_2, x_1) = K(x_1, x_2)$], its eigenfunctions v_n corresponding to distinct eigenvalues γ_n are orthogonal in the interval $(-a,a)$; that is (Ref. 5, p. 413),

$$\int_{-a}^{a} v_m(x) v_n(x)\, dx = 0, \qquad m \neq n. \tag{5}$$

It should be noted that the eigenfunctions are in general complex and are defined over the surface of the mirrors only. They are not orthogonal in the power (Hermitian) sense as commonly encountered in lossless systems. Here, the system is basically a lossy one and the orthogonality relation is

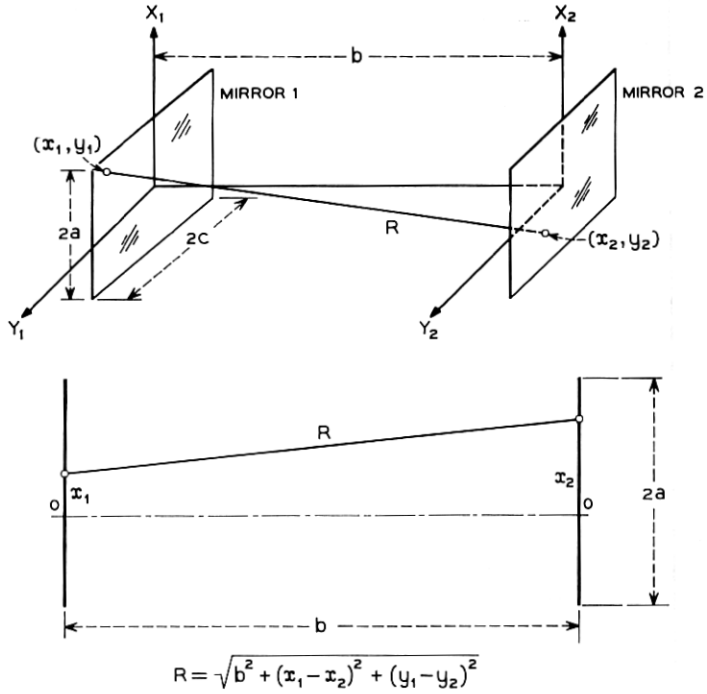

Fig. 2 — Geometry of rectangular plane mirrors.

one which is generally applicable to lossy systems, such as lossy-wall waveguides.

The eigenfunctions are distribution functions of the field over mirror surfaces and represent the various normal modes of the system. The normal modes for rectangular plane mirrors are obtained by taking the products of the normal modes for infinite strip mirrors in x and y directions; that is,

$$v_{mn}(x,y) = v_{x,m}(x)v_{y,n}(y). \tag{6}$$

We designate this as the TEM_{mn} mode for the rectangular plane-mirror interferometer. In view of (5) we see that the normal mode distribution functions v_{mn} are orthogonal over the surface of the rectangular mirror.

The logarithms of the eigenvalues represent propagation constants associated with the normal modes. The propagation constant for the TEM_{mn} mode of rectangular plane mirrors is given by

$$\log \gamma_{mn} = \log \gamma_{x,m} + \log \gamma_{y,n}\,. \tag{7}$$

The real part of the propagation constant specifies the loss per transit

and the imaginary part the phase shift per transit, in addition to the geometrical phase shift, for the normal modes.

2.3 *Circular Plane Mirrors*

It is shown in Appendix B that the solutions to the integral equation for circular plane mirrors (Fig. 3) when $a^2/b\lambda$ is much less than $(b/a)^2$, are given by

$$v(r,\varphi) = R_n(r)e^{-jn\varphi} \qquad (n = \text{integer}), \tag{8}$$

where $R_n(r)$ satisfies the reduced integral equation

$$R_n(r_2)\sqrt{r_2} = \gamma_n \int_0^a K_n(r_2, r_1)R_n(r_1)\sqrt{r_1}\, dr_1, \tag{9}$$

with

$$K_n(r_2, r_1) = j^{n+1}\frac{k}{b} J_n\left(k\frac{r_1 r_2}{b}\right)\sqrt{r_1 r_2}\, e^{-jk(r_1^2+r_2^2)/2b}, \tag{9a}$$

where J_n is a Bessel function of the first kind and nth order. As in the

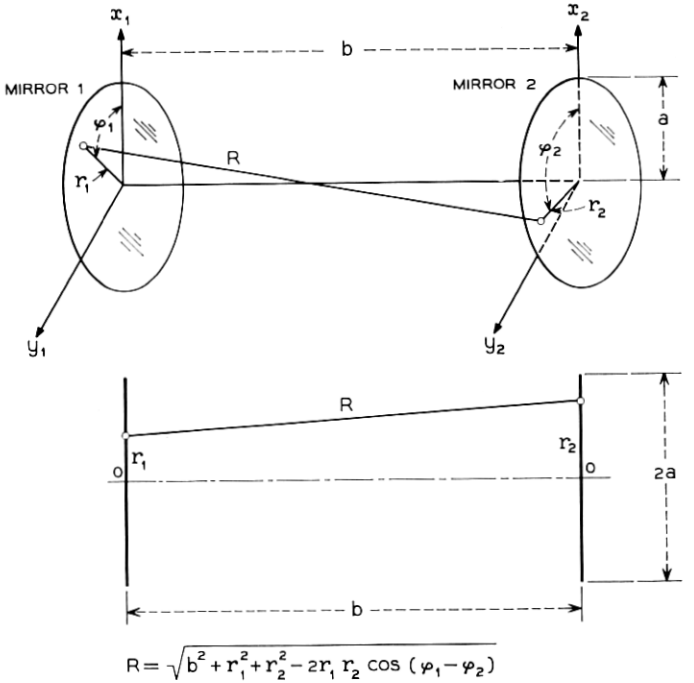

Fig. 3 — Geometry of circular plane mirrors.

problem of infinite strip mirrors, (9) is a homogeneous linear integral equation of the second kind with a continuous and symmetric kernel. Its eigenfunctions corresponding to distinct eigenvalues are orthogonal in the interval $(0,a)$; that is,

$$\int_0^a R_{nl}(r)R_{nm}(r)r\,dr = 0, \qquad (l \neq m). \tag{10}$$

Therefore, we see that the distribution functions $v_{nm}(r,\varphi) = R_{nm}(r)e^{-jn\varphi}$ corresponding to distinct eigenvalues γ_{nm} are orthogonal over the surface of the mirror; that is,

$$\int_0^{2\pi}\int_0^a v_{nm}(r,\varphi)v_{kl}(r,\varphi)r\,dr\,d\varphi = 0 \qquad (\text{either } n \neq k \text{ or } m \neq l). \tag{11}$$

The set of eigenfunctions R_{nm} describes the radial variations of field intensity on the circular mirrors, and the angular variations are sinusoidal in form. We designate a normal mode of the circular plane mirrors as the TEM_{nm} mode, with n denoting the order of angular variation and m denoting the order of radial variation. The propagation constant associated with the TEM_{nm} mode is simply $\log \gamma_{nm}$, which must be obtained from the solution of (9).

2.4 *Confocal Spherical or Paraboloidal Mirrors*

A number of geometries other than plane parallel mirrors have been suggested, and it is believed that most of these can be studied using the same iterative technique. One of the geometries we investigated is that of a confocal spherical system.[6] In this geometry the spherical mirrors have identical curvatures and their foci are coincident, as shown in Fig. 4. One of the possible advantages of such a system is the relative ease of adjustment, since the mirrors are no longer required to be parallel as in the case of the parallel plane system. Another is that the focusing action of the mirrors might give rise to lower diffraction losses.

A spherical mirror with a small curvature approximates closely a paraboloidal mirror. In the case of confocal spherical mirrors, the conditions that its curvature be small is equivalent to saying that the separation between mirrors is large compared to the dimensions of the mirrors. It is shown in Appendix C that the solutions to the integral equation for confocal paraboloidal mirrors, when $a^2/b\lambda$ is much less than $(b/a)^2$, are given by

$$v(r,\varphi) = S_n(r)e^{-jn\varphi} \qquad (n = \text{integer}), \tag{12}$$

where $S_n(r)$ satisfies the reduced integral equation

$$S_n(r_2)\sqrt{r_2} = \gamma_n \int_0^a K_n(r_2, r_1) S_n(r_1)\sqrt{r_1}\, dr_1, \tag{13}$$

with

$$K_n(r_2, r_1) = j^{n+1}\frac{k}{b} J_n\left(k\frac{r_1 r_2}{b}\right)\sqrt{r_1 r_2}. \tag{13a}$$

Again, we see that (13) is a homogeneous linear integral equation of the second kind with a continuous and symmetric kernel. Therefore, general remarks concerning the normal modes of circular plane mirrors given in the foregoing section are also applicable to confocal spherical or paraboloidal mirrors.

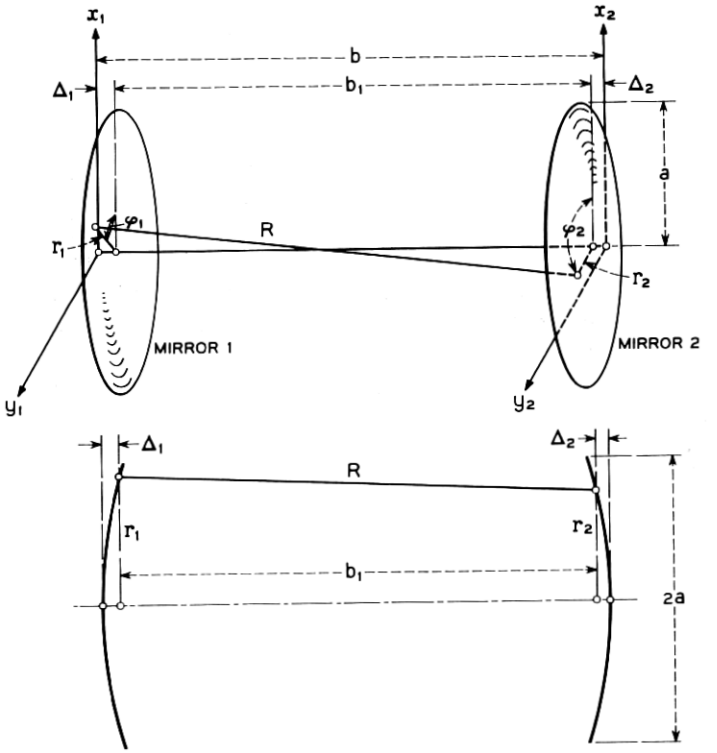

$$R = \sqrt{b_1^2 + r_1^2 + r_2^2 - 2r_1 r_2 \cos(\varphi_1 - \varphi_2)}$$

$$\Delta_1 = b - \sqrt{b^2 - r_1^2}$$

$$\Delta_2 = b - \sqrt{b^2 - r_2^2}$$

Fig. 4 — Geometry of confocal spherical mirrors.

III. COMPUTER SOLUTIONS

3.1 *General*

An IBM 704 computer was programmed to solve the integral equations for the various geometries of the interferometer by the method of successive approximations. As mentioned previously, this is analogous to the physical process of launching an initial distribution of wavefront in the interferometer and letting it bounce to and fro between the mirrors.

3.2 *Infinite Strip Mirrors*

The first problem put on the computer was that of a pair of infinite strip mirrors, having the dimensions $2a = 50\lambda$, $b = 100\lambda$. Equation (26) was employed for the computation, using an initial excitation of a uniform plane wave at the first mirror. A total of one hundred increments was used for the numerical integration. After the first transit the field intensity (electric or magnetic) had the amplitude and phase shown in Fig. 5. In these and subsequent amplitude and phase distributions the curves are normalized so that the maximum amplitude is unity, and the phase at that point is zero. The large ripples are due to the fact that the initial wave front contains 6.25 Fresnel zones as seen from the center of the second mirror. Therefore, in passing from the center to the edge of the second mirror there is a change of 3×6.25 Fresnel zones, and this agrees with the number of reversals in curvature seen in the amplitude distribution.

With subsequent transits, these ripples grow smaller, the amplitude at the edge of the mirror decreases, and the relative field distributions approach a steady state. By the time the wave had made three hundred bounces, the fluctuations occurring from bounce to bounce were less than 0.03 per cent of the final average value. The amplitude and phase for the 300th bounce are also shown in Fig. 5.

We regard this field distribution as an iterative normal mode of the interferometer. In other words, if this distribution is introduced as an initial wave at one mirror it will reproduce the same distribution at the other mirror. Indeed, this is what the computer is verifying when we compute the 301st bounce.

Once the solutions have reached a steady state, we can pick any point on the wavefront, say the center of the mirror, and examine how the absolute phase and amplitude change from bounce to bounce. In this way we determined that the power loss of this mode is 0.688 per cent per transit and the phase shift per transit has a lead of 1.59 degrees.

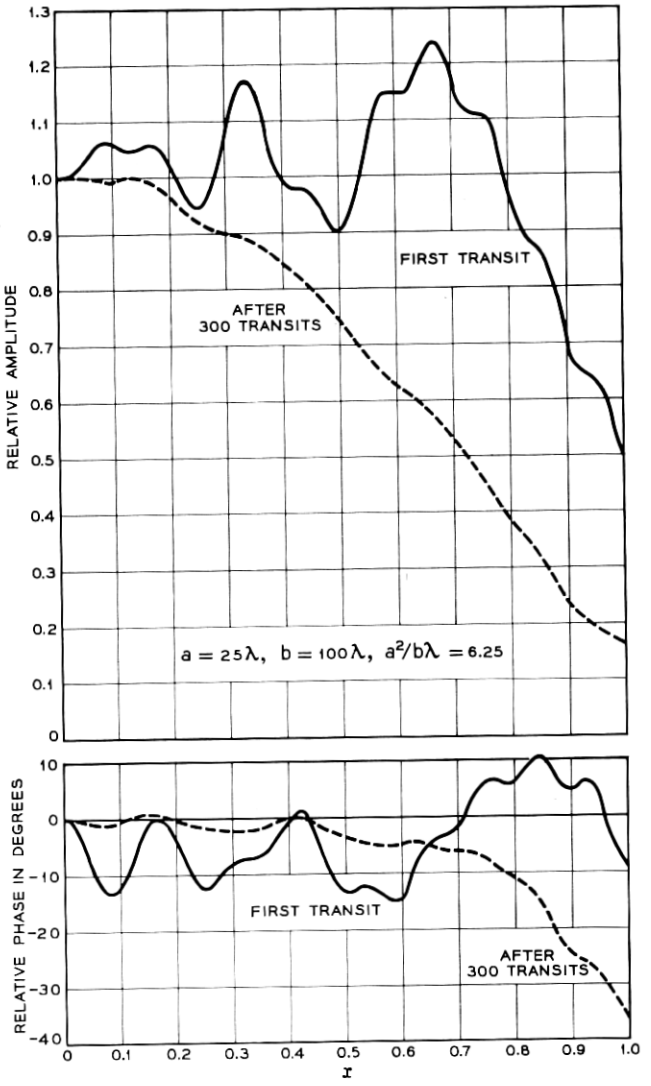

Fig. 5 — Relative amplitude and phase distributions of field intensity for infinite strip mirrors. (The initially launched wave has a uniform distribution.)

Since phase shift is measured relative to the free-space electrical length between the mirrors (360 b/λ degrees), this means that the mode has an effective phase velocity which is slightly greater than the speed of light, just as for a metal tube waveguide.

In Fig. 6 is shown how the field intensity at an arbitrary off-center

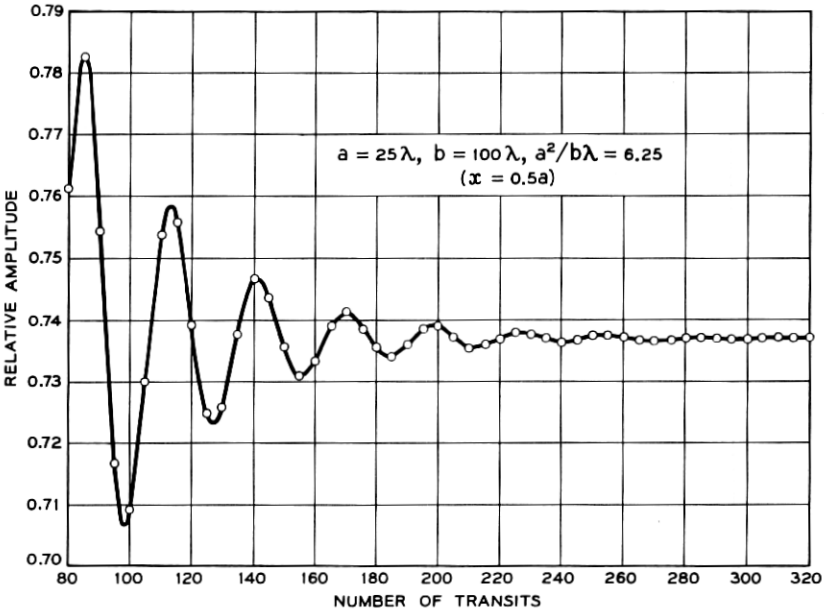

Fig. 6 — Fluctuation of field amplitude at $x = 0.5$ as a function of number of transits. (The initially launched wave has a uniform distribution.)

point ($x = 0.5a$) approaches its steady-state normalized value after a start from a uniform plane wave. After the 100th transit the plot appears to be a damped sine wave. We interpret this damped oscillation as the beating between two normal modes having different phase velocities. The mode with the lower attenuation, of course, survives the longest, and this is the one shown in Fig. 5. We regard this as the dominant mode of the interferometer. We believe the other mode which beats with the dominant mode to be the next-higher order, even-symmetric mode. Prior to the 100th transit, the curve is irregular, indicating that a number of still higher order modes are present which are damped out rapidly.

The next step in the infinite strip problem was to repeat solutions of the above type for other sets of dimensions. However, if $a^2/b\lambda$ is very small compared to $(b/a)^2$, the actual dimensions of the mirrors and their spacing are no longer important, the only parameter of importance being the Fresnel number $N = a^2/b\lambda$. This is approximately equal to the number of Fresnel zones seen in one mirror from the center of the other mirror, and as pointed out earlier, it determines the number of ripples in the field distributions. Amplitude and phase distributions for the

dominant mode obtained by solving (27) are shown in Fig. 7 for different values of N. The larger the N, the weaker is the field intensity at the edge of the mirror, and the smaller is the power loss due to spill-over. The plot of power loss per transit as a function of N is approximately a straight line on log-log paper and is shown as the lowest line in Fig. 8. The phase shift per transit as a function of N is given by the lowest line in Fig. 9.

A uniform plane wave excitation can never give rise to a mode with odd symmetry. In order to investigate the possibility of modes of this

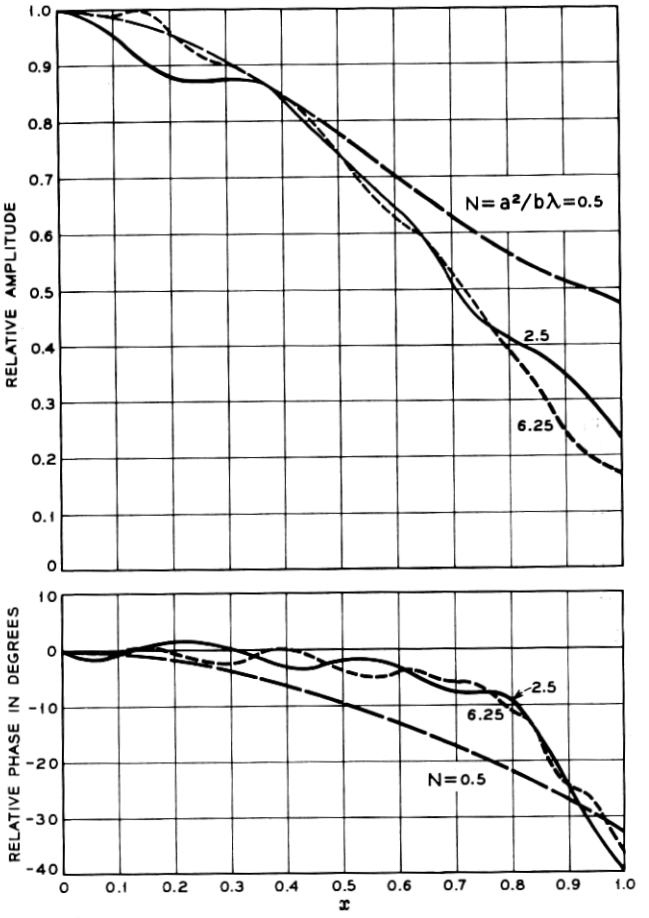

Fig. 7 — Relative amplitude and phase distributions of field intensity of the lowest order even-symmetric mode for infinite strip mirrors.

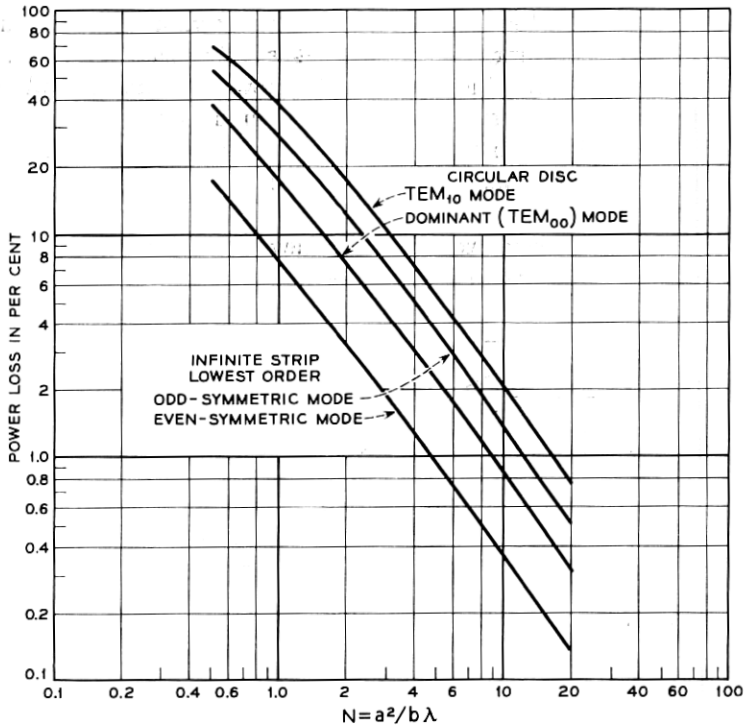

Fig. 8 — Power loss per transit vs. $N = a^2/b\lambda$ for infinite strip and circular plane mirrors.

type, the problem was re-programmed for an initial wave for which the field intensity over one-half the strip (0 to $+a$) was equal but opposite in sign to the field intensity over the other half of the strip (0 to $-a$). Steady-state solutions did indeed result, and odd-symmetric normal modes therefore exist. The amplitude and phase distributions are shown in Fig. 10 for several values of N. The amplitude is zero at the center, as expected. While shown for only one half of the strip, it is the same in the other half, but with a reversal in sign. Note that for the same values of N, the amplitude at the edge is higher than for the dominant mode. The spill-over loss should be higher and this is confirmed by the loss curve in Fig. 8 labeled "infinite strip odd-symmetric mode." The corresponding phase shift curve is shown in Fig. 9.

3.3 *Circular Plane Mirrors*

The feasibility of obtaining the normal mode solutions for the infinite strip mirrors having been established, programs were next set up to

investigate the modes for plane circular mirrors. The first case considered was that for uniform plane wave excitation of the system. Once again, the polarization was assumed to be everywhere parallel to the same axis, and this results in a scalar wave solution having circular symmetry [(9) with $n = 0$]. That is, the amplitude and phase of the field intensity is the same for all points at the same radius from the center. The transverse field distributions for the lowest order mode of this type are shown in Fig. 11 for various values of N. The loss and phase shift are shown in Figs. 8 and 9 under the title "circular disc (dominant mode, TEM_{00})." One hundred increments along the radius were used for the numerical integrations involved.

Next we examined modes of the odd-symmetric type for circular plane mirrors. The equation we used was (9) with $n = 1$. Fig. 12 shows amplitude and phase distributions for the lowest order mode of the odd-symmetric type for circular plane mirrors. Again the loss and phase

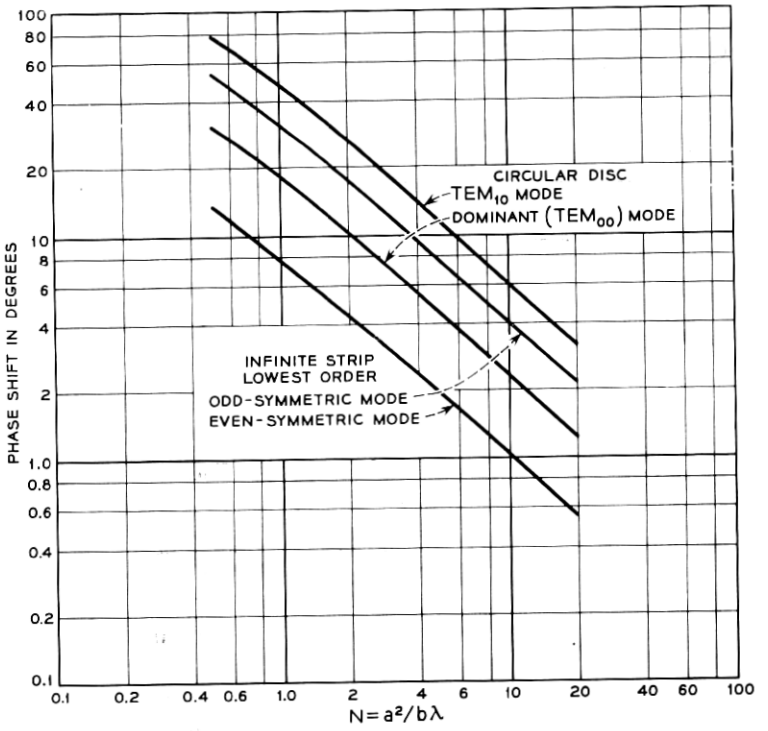

Fig. 9 — Phase shift per transit (leading relative to geometrical phase shift) vs. $N = a^2/b\lambda$ for infinite strip and circular plane mirrors.

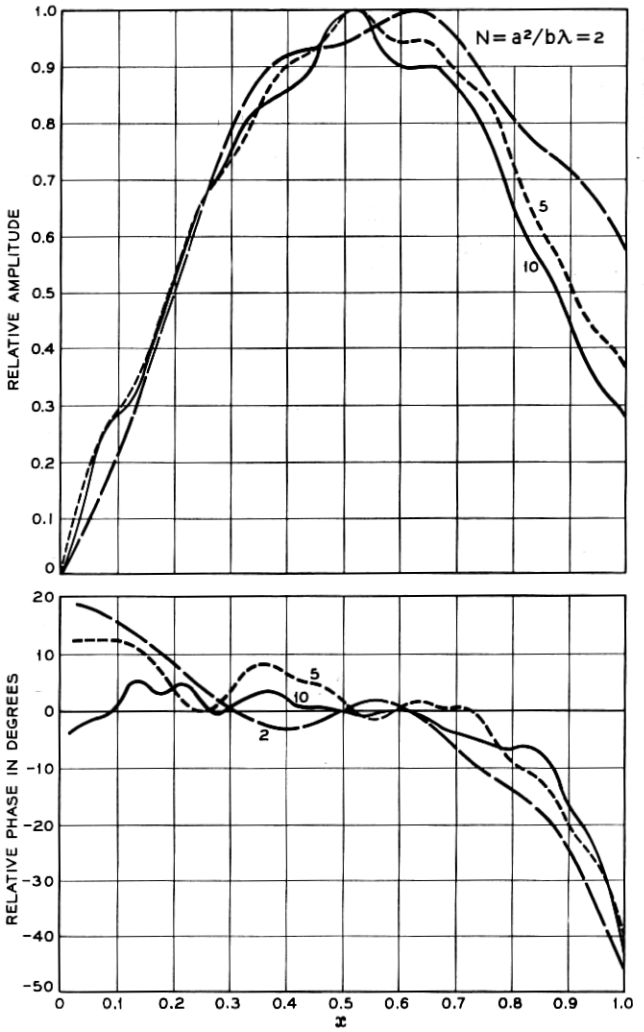

Fig. 10 — Relative amplitude and phase distributions of field intensity of the lowest-order odd-symmetric mode for infinite strip mirrors.

shift are given in Figs. 8 and 9 under the title "circular disc, TEM_{10} mode."

Normal modes with higher orders of angular variation ($n \geqq 2$) and radial variation ($m \geqq 1$) have greater losses and phase shifts than those of TEM_{00} and TEM_{10} modes. The mode with the least attenuation is

therefore the lowest order, of TEM_{00} mode, which we designate as the dominant mode for circular plane mirrors.

3.4 *Confocal Spherical Mirrors*

Before (13) was programmed for solutions on the computer a more general method for solving the problem of the confocal spherical mirrors

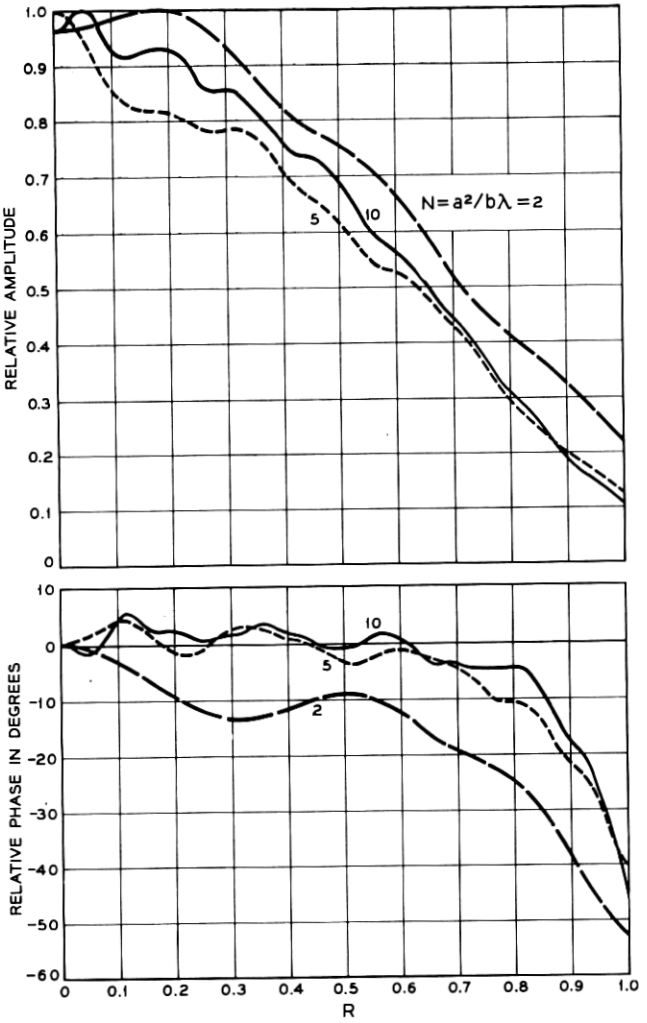

Fig. 11 — Relative amplitude and phase distributions of field intensity of the dominant (TEM_{00}) mode for circular plane mirrors.

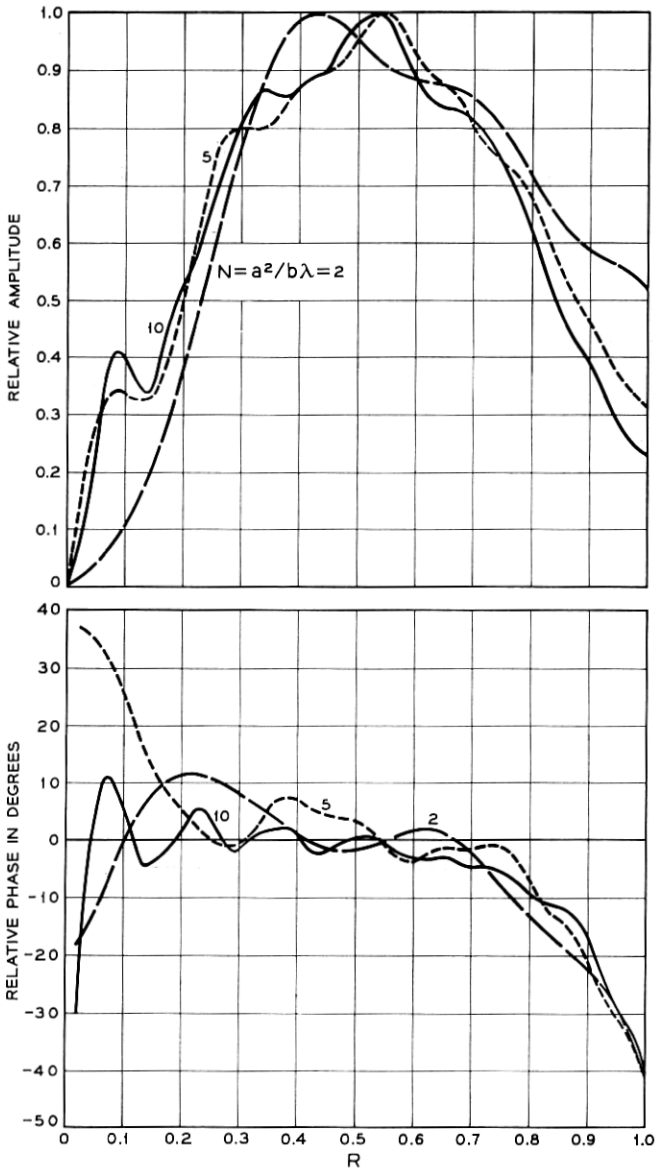

Fig. 12 — Relative amplitude and phase distributions of field intensity of the TEM_{10} mode for circular plane mirrors.

was tried — a procedure that can be used to solve problems involving mirrors with rather arbitrary but small curvatures. In this method the field at each mirror is calculated using the equation for circular plane mirrors and then a phase distribution corresponding to the curvature of the mirror is added to this field before it is used in the next iterative computation. The results from this general method of solution and from solving (13) are in perfect agreement.

The problem of confocal spherical mirrors has also been solved by Goubau[8] and Boyd and Gordon.[9] The results of their analyses are in good agreement with our computed results.

Amplitude distributions of the field intensity for TEM_{00} and TEM_{10} modes are shown in Figs. 13 and 14. The phase distributions are all uniform over the surface of the mirrors and therefore are not plotted. The loss and phase shift per transit are given in Figs. 15 and 16. We note some rather remarkable differences between these solutions and those obtained for circular plane mirrors. First, the field is much more tightly concentrated near the axis of the reflector and falls to a much lower value at the edge than is true for plane mirrors; also the amplitude distribution does not have ripples in it, but is smooth. Second,

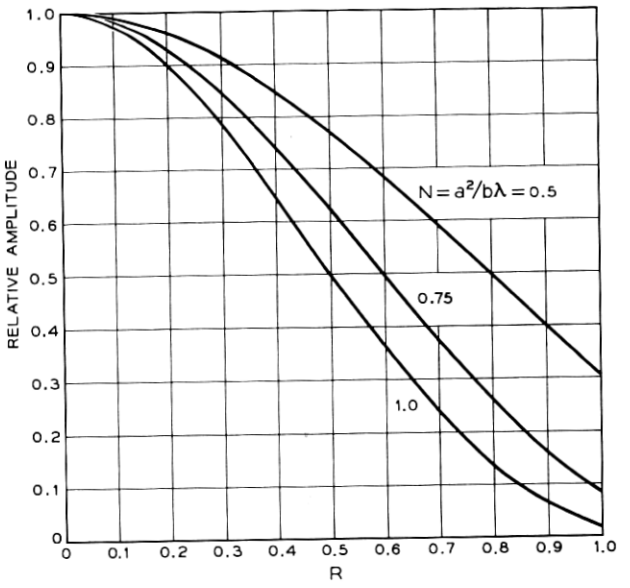

Fig. 13 — Relative amplitude distribution of field intensity of the dominant (TEM_{00}) mode for confocal spherical mirrors. The relative phase distribution on the surface of the mirror is uniform.

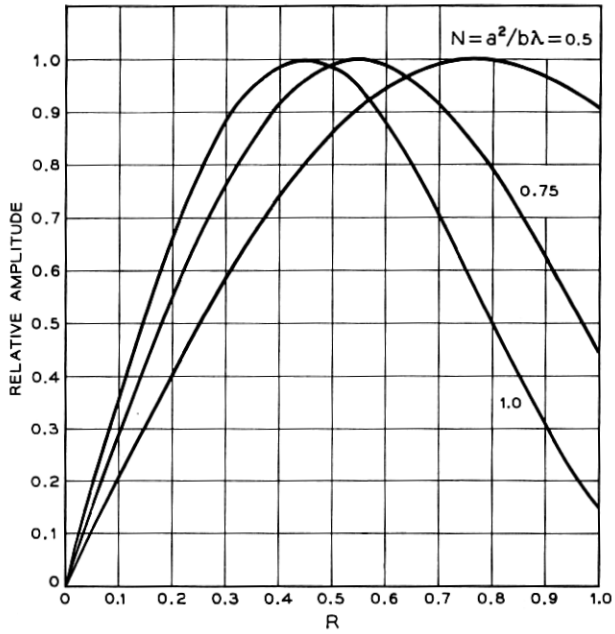

Fig. 14 — Relative amplitude distribution of field intensity of the TEM_{10} mode for confocal spherical mirrors. The relative phase distribution on the surface of the mirror is uniform.

the surface of the reflector coincides with the phase front of the wave, making it an equiphase surface. Third, the difference between the phase shifts for all the normal modes are integral multiples of 90 degrees. Fourth, the losses may be orders of magnitude less than those for plane mirrors.

The result that the mirror surface is an equiphase surface should not be surprising, but can be deduced from integral equation (13). If we associate the factor j^{n+1} with γ_n the kernel becomes real. Since the eigenvalues and eigenfunctions of a real symmetric kernel are all real,[7] we see that the field distribution is of uniform phase over the surface of the mirror. Furthermore, since $(j^{n+1}\gamma_n)$ is real, the phase shift for the normal modes belonging to a set of modes with a given angular variation must be an integral multiple of 180 degrees and the difference between the phase shifts for the normal modes with different angular variations but the same radial variation is an integral multiple of 90 degrees; that is, the phase shift is equal to $[180m + 90(n + 1)]$ degrees. Therefore, if the mirrors are adjusted for the resonance of a particular normal mode,

half of the totality of all the modes are also resonant. However, the resonant mode with the lowest loss would persist longest in the resonator. Just as in the case of plane parallel mirrors, the mode with the lowest loss is the TEM_{00} mode.

IV. DISCUSSION OF RESULTS

The results of machine computation have shown that a two-mirror interferometer, whether of the plane or concave mirror type, can have

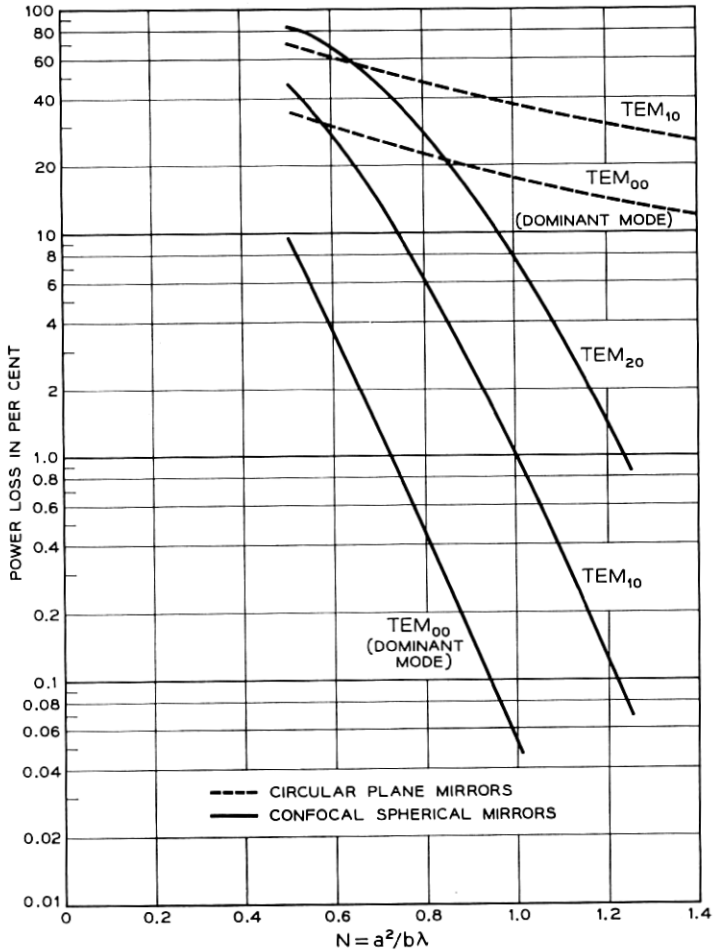

Fig. 15 — Power loss per transit vs. $N = a^2/b\lambda$ for confocal spherical mirrors. (Dashed curves for circular plane mirrors are shown for comparison).

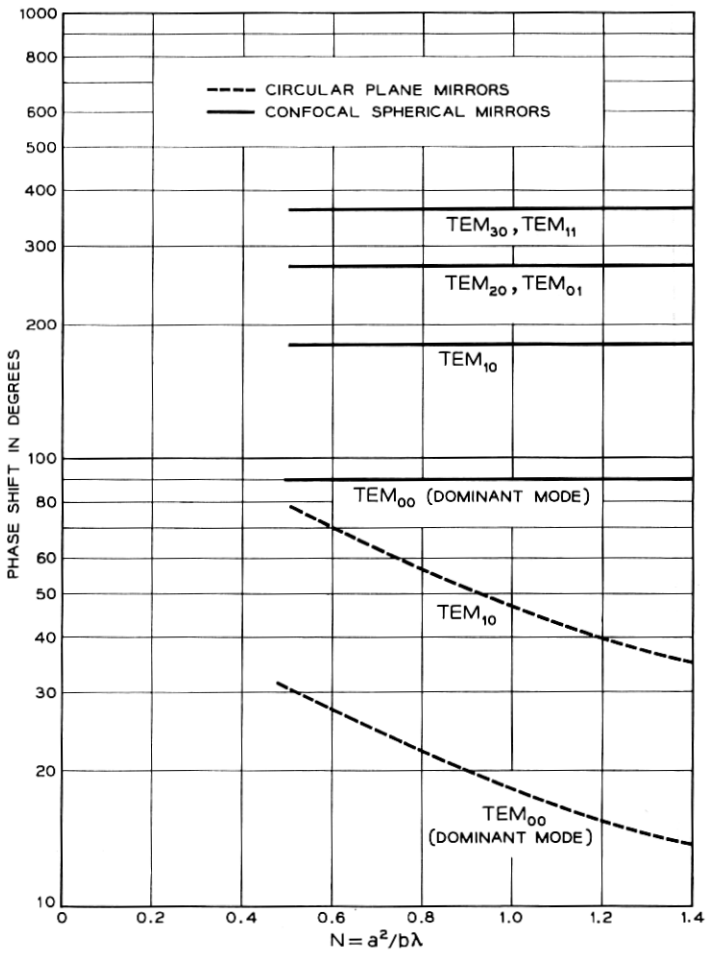

Fig. 16 — Phase shift per transit (leading relative to geometrical phase shift) vs. $N = a^2/b\lambda$ for confocal spherical mirrors. (Dashed curves for circular plane mirrors are shown for comparison.)

normal modes of propagation which are self-perpetuating or self-reproducing in the distance of one transit. We use the term mode of propagation rather than mode of resonance to emphasize the fact that these steady-state solutions are the result of multiple transits whether or not the plate separation happens to be adjusted for resonance. An analog of the plane mirror interferometer is a transmission medium consisting of a series of periodic collinear apertures, as was shown in Fig. 1. The same

solutions apply, and here it is clear that the reproduction of a normal mode field at successive apertures does not depend on any critical relation between b and λ.

In Fig. 17 is shown the way in which a number of square-plate modes can be synthesized from the infinite-strip modes. Diagram A shows schematically the field distribution for the dominant square-plate mode obtained as the product of the field distributions of two even-symmetric strip modes crossed at right angles and with polarization as shown. Since the eigenvalue for the square plate is the product of the eigenvalues for the two strips, the phase shift per transit is the sum of the

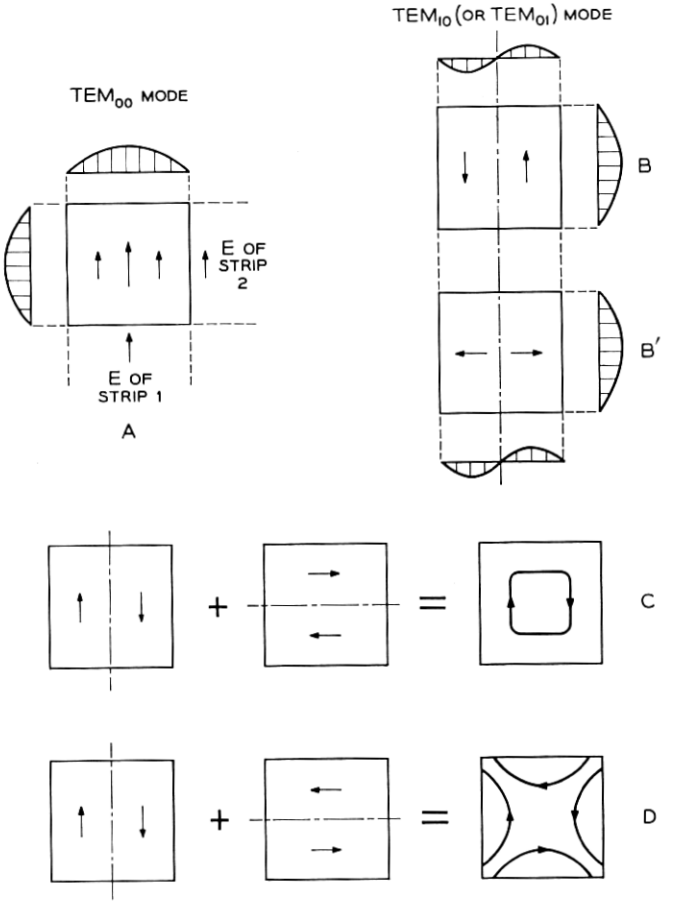

Fig. 17 — Synthesis of normal modes for square mirrors.

phase shifts for the two strips and, if the loss is small, the loss per transit is essentially the sum of the losses for the two strips. Diagram B represents an odd-symmetric square-plate mode formed by taking the product of an even- and an odd-symmetric strip mode; B′ is the same mode but with the polarization rotated 90°; C is a circular electric type of mode formed by *adding* two modes of the type B. This addition is permitted because the two components are degenerate. It follows that the circular electric mode C is degenerate with B and has the same loss and phase shift per transit. By taking the difference between the same two B modes as shown, the mode D is obtained, resembling the TE_{21} mode in circular waveguide. We give all the patterns B, B′, C and D the same designation, TEM_{10} (or TEM_{01}), since they are composites of the one basic mode type. Similar syntheses can be performed for circular mirrors, either plane or concave. It is interesting that degeneracies of this type are common for the interferometer because the electric vector E is at liberty to be parallel or perpendicular to the mirror edges. In a metal waveguide they are uncommon because the polarization of E at the boundaries is restricted.

The dominant mode and a number of higher-order modes for square and circular mirrors are depicted in Fig. 18, in which electric field vectors are shown. This classification of modes applies to plane as well as confocal spherical mirrors. In the case of rectangular mirrors, the x axis may be taken along the longer dimension, in which case the first sub-

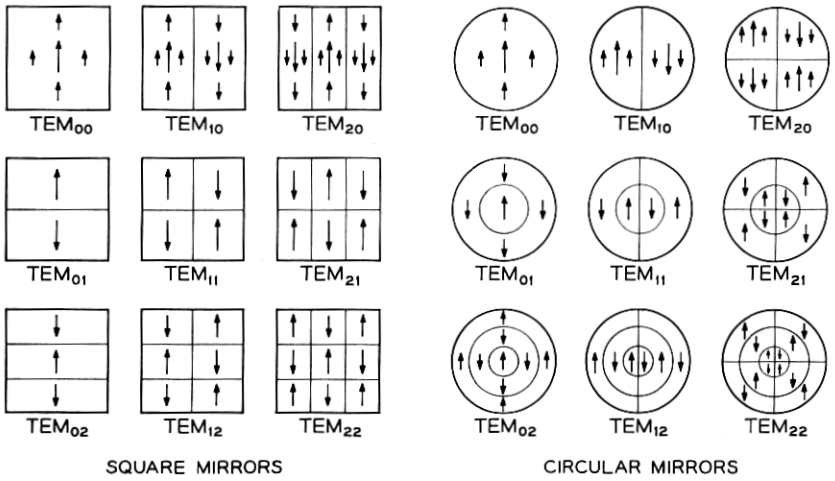

Fig. 18 — Field configuration of normal modes for square and circular mirrors.

script always denotes the number of field reversals along the longer dimension.

In formulating the problem we have assumed that the waves were almost transverse electromagnetic. The solutions for the flat mirror are consistent with this assumption. At the edges of the mirror there is a phase lag of approximately 45 degrees relative to the center, but this is only one-eighth of a wavelength out of many wavelengths for the mirror diameter. Thus the curvature of the wavefront away from the transverse plane is exceedingly small, and the assumption appears justified. For higher-order modes such as B′ of Fig. 17, it is clear that the field lines must have longitudinal components. This is illustrated by an edge view in Fig. 19. However, provided the width of a cell c is much greater than a half-wavelength, the longitudinal field intensity should be negligible compared to the transverse. Only for very high-order modes should this approximation begin to fail. Because the low-order modes of importance are essentially transverse electromagnetic, they are designated as TEM modes.

The plane mirror modes have a phase which is not constant over the mirror. This does not mean that it is impossible to space the mirrors for resonance of the entire field pattern. Actually, the phase delay for one transit is the same for every point on the wavefront. Therefore, if the plates are separated by the distance b plus an additional amount for the phase shift per transit of the mode desired, that mode should resonate in

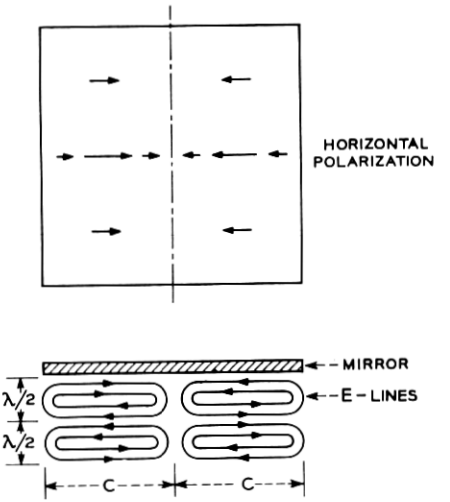

Fig. 19 — Field configuration of the TEM_{10} mode for square mirrors.

the interferometer. Other modes should not be resonant for this separation because they have different phase shifts per transit.

Since the field configurations of many of the normal modes of the interferometer are very similar to those of metal tube and parallel-plane waveguides, it is not surprising to find that simple waveguide theory can be used to predict certain characteristics of the interferometer modes. One of these characteristics is phase shift per transit. For instance, the field distributions of the normal modes for infinite strip mirrors are very similar to those of the TE modes of parallel-plane waveguide; also, by adding two orthogonally polarized TEM_{10} modes for circular plane mirrors, one obtains a field configuration which is very similar to that of the circular electric (TE_{01}) mode of circular waveguide (Fig. 20). Thus the amount of phase shift per transit computed for these modes of the interferometer agrees well with the phase shifts obtained for TE modes of parallel-plane waveguide and TE_{01} mode of circular waveguide. This is illustrated in Fig. 21. We see that agreement becomes better for larger values of N. This is because the similarity between field configurations becomes closer for larger values of N.

If we regard a uniform plane wave as being resolvable into a set of normal modes, there can be no such thing as a resonance for a uniform plane wave. Why then does it appear that there is such a resonance in passive optical interferometers? It is because for the usual optical case $a^2/b\lambda$ is in the thousands. The phase shifts per transit are extremely small, hence the mode resonances lie very close together in frequency. At the same time, the reflection coefficients of the best optical mirrors are so poor, and the Q of the interferometer is so low, that the resonance

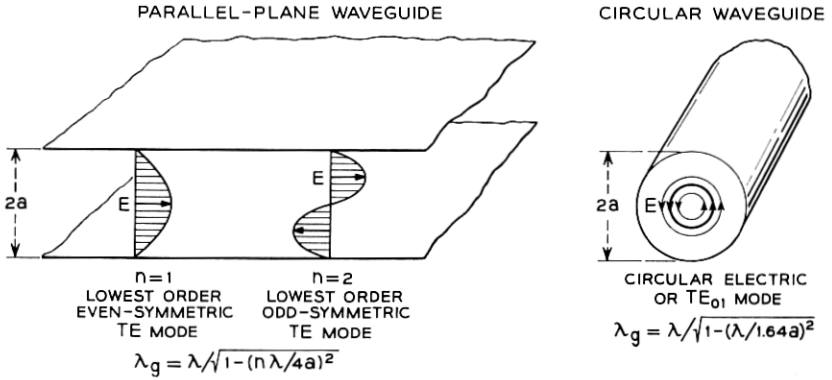

Fig. 20 — TE modes in a parallel-plane waveguide and circular electric mode in a circular waveguide.

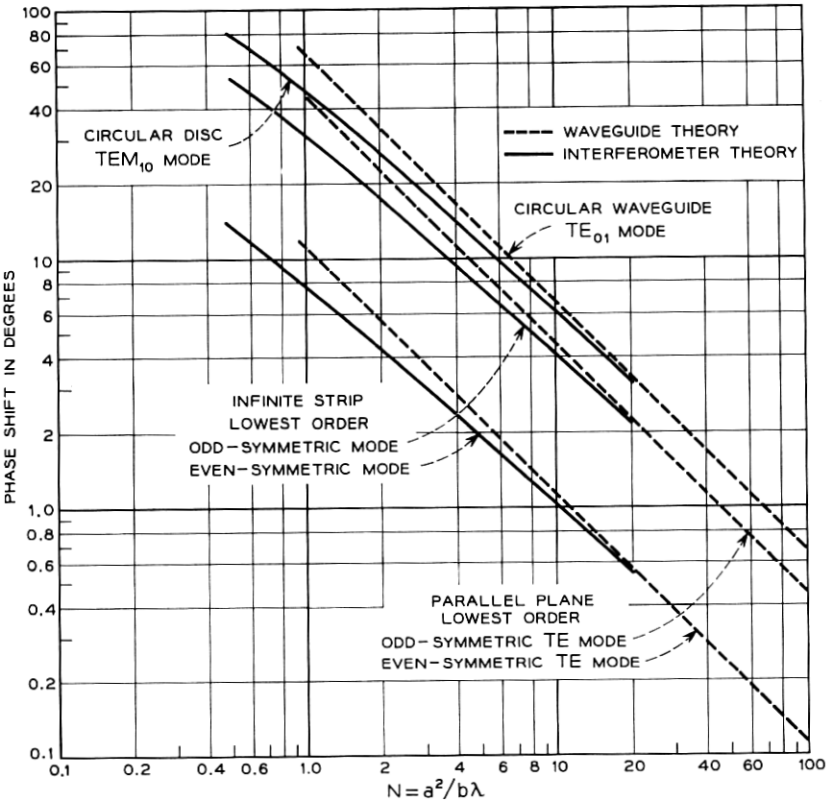

Fig. 21 — Comparison of computed phase shifts based on waveguide theory and on interferometer theory.

line width contains hundreds of normal mode resonances. Thus the uniform plane wave undergoes very little decomposition when resonated. Nevertheless, in the case of an active interferometer, the decomposition may be complete.

We now make use of the formula for the Q of a resonant waveguide cavity to compute the Q of an interferometer system. The Q of a resonant waveguide cavity is given by

$$Q = \frac{|R_1 R_2 e^{-2ab}|}{1 - |R_1 R_2 e^{-2ab}|} \left(\frac{2\pi b}{\lambda_g}\right) \left(\frac{\lambda_g}{\lambda}\right)^2, \tag{14}$$

where α is the attenuation constant of the waveguide and λ_g is the guide wavelength. For the interferometer we assume that α is zero and that λ_g is equal to λ, the free-space wavelength. The voltage reflection coeffi-

cients R_1 and R_2 for the two reflectors are given by

$$|R_1| = |R_2| = \sqrt{1 - \delta_r - \delta_d}, \tag{15}$$

where δ_r is the power loss in reflection and δ_d is the power loss due to spill-over. When these losses are very small, Q reduces to

$$Q \cong \frac{1}{\delta_r + \delta_d} 2\pi \frac{b}{\lambda}. \tag{16}$$

Hence

$$\frac{1}{Q} = \frac{1}{Q_r} + \frac{1}{Q_d}, \tag{17}$$

where

$$Q_r = \frac{2\pi b}{\lambda \delta_r}, \qquad Q_d = \frac{2\pi b}{\lambda \delta_d}. \tag{18}$$

The resonance line width at half-power points given as the change in electrical length of the resonator, $\Delta\varphi$, is

$$\begin{aligned} \Delta\varphi &= 2\pi \left(\frac{b}{\lambda}\right)\left(\frac{\Delta\lambda}{\lambda}\right) \\ &= \delta_r + \delta_d \text{ radians}, \end{aligned} \tag{19}$$

where we have substituted $(1/Q)$ for $(\Delta\lambda/\lambda)$.

Let us consider an interferometer having circular plane mirrors with $2a = 1$ cm, $b = 20$ cm, $\lambda = 5 \times 10^{-5}$ cm and a reflection loss of $\delta_r = 0.02$. In this case $N = a^2/b\lambda = 250$. Extrapolating the loss and phase shift curves of Figs. 8 and 9, we obtain diffraction loss $\delta_d = 9 \times 10^{-5}$ and phase shift for the dominant (TEM_{00}) mode $\varphi_d = 0.11$ degree. The diffraction loss is thus negligible compared to reflection loss, which limits the Q to a value of 1.25×10^8. The phase shift for the next higher order (TEM_{10}) mode is 0.30 degree and therefore it is separated from the dominant (TEM_{00}) mode by 0.19 degree or 0.0033 radian. The resonance line width, as given by (19), is 0.02 radian. Thus we see that TEM_{00} and TEM_{10} modes are not resolved. As the mirror separation is reduced or mirror size increased, more and more normal modes will become unresolved and a uniform plane wave will suffer less decomposition when resonated.

When an interferometer is filled with an active medium, the medium can compensate for the mirror losses and yield an enormously increased Q. Under these circumstances, the modes may be clearly resolved, and their Q's will be determined by the diffraction losses. If the gain of the

medium is increased until it compensates for mirror losses plus the diffraction loss of the lowest order mode, that mode will become unstable and oscillation can result. All higher-order modes will be stable and have positive net loss. If the gain of the medium is further increased, then many modes may become unstable. In starting from a quiescent condition, spontaneous emission can initiate a large number of characteristic waves in the interferometer. These may then start to grow, but the dominant mode will always grow faster and should saturate first. At saturation the steady-state field distribution will be considerably altered. The relative field at the edges of the mirrors should increase, thereby increasing the relative power loss. This can be described as a coupling of power into other modes as a result of the nonlinearity of the medium. No attempt has yet been made to analyze this situation. The linear theory is at present of most interest because it allows the computation of the starting conditions for oscillation.

With the development of the normal mode picture of interferometer operation and the computation of the losses for these modes, we may now ask if there is an optimum geometry for a maser interferometer which will permit oscillation for the lowest possible gain in the medium. We know that the power gained from the medium can be increased by increasing length. For very great lengths corresponding to the far-field region ($N < 0.1$), the power gained from the medium increases more rapidly than transmission loss as length is increased, and there must always be some length beyond which oscillations can occur. However, these lengths are too great to be of practical interest. In the near-field region ($N > 1$), represented by the curves of Fig. 8, the diffraction loss increases more rapidly than the medium gain. Therefore, if the reflection loss is sufficiently small, an optimum length may exist which is most favorable for oscillation.

To be more specific, let us consider a circular plane mirror interferometer. From Fig. 8 we find that the loss for the dominant mode may be represented by the expression

$$\delta_d = 0.207 \left(\frac{b\lambda}{a^2}\right)^{1.4}. \tag{20}$$

In order to find the optimum value of b to give a maximum Q, (20) and (18) are substituted in (17) and the resulting equation is differentiated with respect to b. For the optimum b, the diffraction loss is 2.5 times the reflection loss, and not equal to it, as might be supposed. Moreover, this result is general and holds for all modes and all shapes of plane mirrors represented in Fig. 8, provided the optimum falls on the straight-line

portions of the loss curves. Since the power supplied by the medium is proportional to the stored energy in the interferometer, while the power loss of the passive interferometer is just ω/Q times the stored energy, oscillation is most likely to occur when Q is a maximum. Fig. 22 illustrates the way the interferometer dimensions affect Q. If a given mirror diameter is chosen (as represented by the dashed line A), there is clearly an optimum distance b which will produce a maximum Q (intersection of lines A and B). However, if the distance b is held constant, there is no optimum value for a. The larger a, the higher will be Q, although it will approach a limiting value beyond which there is nothing to be gained by further increase of a.

As an example, let us assume a case where

$$\lambda = 10^{-4} \text{ cm},$$

$$2a = \text{plate diameter} = 2 \text{ cm},$$

$$\delta_r = \text{power reflection loss} = 0.001.$$

The optimum proportions require that δ_d be 0.0025, and for this, b is 435 cm and the resulting Q is 7.8×10^9. The length of 435 cm is probably impractically large for a maser. If b is reduced to a more reasonable value of 50 cm, the Q will drop to 3.14×10^9, which is the limiting value due to reflection loss. (The value assumed here for δ_r is already much lower than can be obtained from evaporated metal films and would require the technique of multilayered dielectric films.) In order to oscillate, the active medium would have to have a power amplification factor in excess of 1.00002 per centimeter of path.

In the case of confocal paraboloidal mirrors of 2 cm diameter, the optimum length turns out to be 8900 cm. If the diameter is reduced to 0.5 cm, the optimum length is still 530 cm, and for these proportions Q is 3.1×10^{10}. It is clear that with confocal mirrors the diffraction losses are negligible for any reasonable proportions of the interferometer.

One question of importance is whether there is an optimum set of dimensions which will discriminate against unwanted modes. It has sometimes been suggested that by making the mirror diameter small relative to the mirror spacing, "slant rays" will be more rapidly lost from the system. However, from Fig. 8 it can be seen that the ratios of the losses for the several modes is independent of N provided N is greater than 1. Thus, if diffraction losses predominate, there is no way of discriminating against unwanted modes by juggling dimensions. The limiting amount of discrimination is merely governed by the ratio of the losses for the different modes, which is independent of the dimensions. However, if reflection losses predominate, the discrimination between

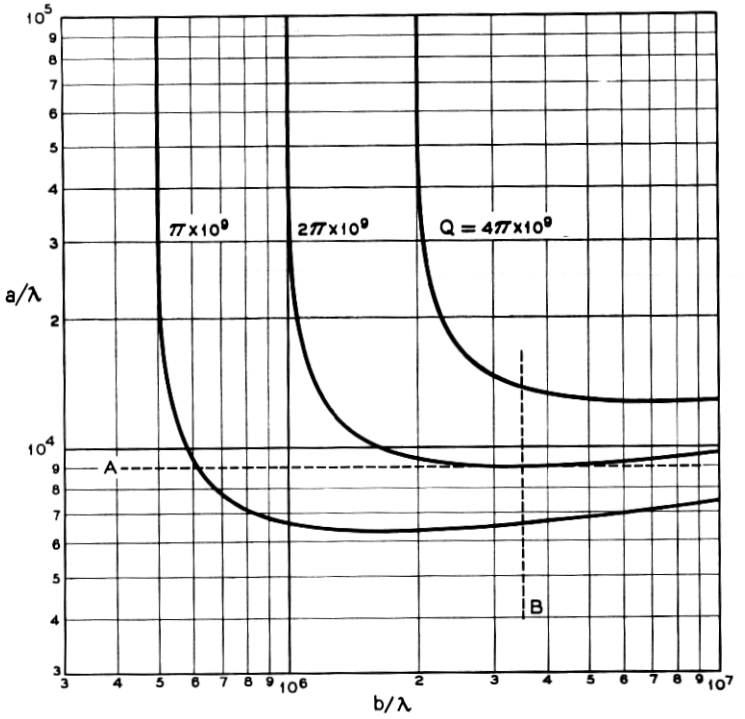

Fig. 22 — Interferometer dimensions for constant Q. (Circular plane mirrors, reflection loss = δ_r = 0.001.)

lower-order modes would be almost nonexistent and it would be advantageous to increase mirror separation and/or decrease mirror dimensions so as to make diffraction losses predominate. In the case of the confocal mirrors, the loss ratios between modes are not constant (Fig. 15) although, for values of N larger than those shown, they may become so. At any rate, for values of N close to unity, a small amount of increased discrimination against higher order modes can be obtained by making the mirrors *larger*.

V. CONCLUSIONS

Diffraction studies carried out on the IBM computer have led to the following conclusions:

1. Fabry-Perot interferometers, whether of the plane or concave mirror type, are characterized by a discrete set of normal modes which can be defined on an iterative basis. The dominant mode has a field intensity which falls to low values at the edges of the mirrors, thereby

causing the power loss due to diffractive spillover to be much lower than would be predicted on the assumption of uniform plane wave excitation.

2. Uniform plane waves are not normal modes for a flat-plate interferometer. Consequently, interferometer resonances do not exist for "slant rays," i.e., plane waves traveling at an angle with respect to the longitudinal axis.

3. The losses for the dominant mode of the plane mirror system are so low that for most practical geometries performance will be limited by reflection losses and scattering due to aberrations. For confocal mirrors the diffraction losses are even lower.

4. There are no higher-order modes with losses lower than the dominant (lowest-order) mode.

5. The ratio of diffraction losses between the modes investigated for the plane mirror system is independent of the interferometer dimensions in the range of interest. Therefore, if diffraction losses predominate, there is no way of proportioning the interferometer so as to favor any one mode.

The computer technique we employed is general and versatile. It can be used for studying mirrors having rather arbitrary but small curvatures. With little modification, the same technique can be used to study the effects of aberration and misalignment.

APPENDIX A

Rectangular Plane Mirrors

The geometry for rectangular plane mirrors parallel to the xy plane is shown in Fig. 2. According to (1), the iterative equation for computing the field at the surface of mirrors is

$$u_{q+1}(x_2, y_2) = \frac{j}{2\lambda} \int_{-c}^{c} \int_{-a}^{a} u_q(x_1, y_1) \frac{e^{-jkR}}{R} \left(1 + \frac{b}{R}\right) dx_1 dy_1, \quad (21)$$

where

$$R = \sqrt{b^2 + (x_1 - x_2)^2 + (y_1 - y_2)^2}.$$

If b/a and b/c are large, (21) can be reduced to

$$u_{q+1}(x_2, y_2) = \frac{je^{-jkb}}{\lambda b} \int_{-c}^{c} \int_{-a}^{a} u_q(x_1, y_1) e^{-jk[(x_1-x_2)^2+(y_1-y_2)^2]/2b} dx_1 dy_1, \quad (22)$$

which is valid for $(a^2/b\lambda) \ll (b/a)^2$ and $(c^2/b\lambda) \ll (b/c)^2$.* The corresponding integral equation is

* Actually, the stringency of this requirement can be relaxed somewhat for lower-order modes in which field intensities near the edges of the mirror are rather low. We have made check computations for the case $a^2/b\lambda = 5$ and $(b/a)^2 = 25$ and have found that the results based on the exact equation and on the approximate equation are in essential agreement.

$$v(x_2, y_2) = \gamma \int_{-c}^{c} \int_{-a}^{a} K(x_2, x_1; y_2, y_1) v(x_1, y_1)\, dx_1 dy_1, \tag{23}$$

where

$$K(x_2, x_1; y_2, y_1) = \frac{j}{\lambda b} e^{-jk[(x_1-x_2)^2+(y_1-y_2)^2]/2b} \tag{23a}$$

and the factor e^{-jkb} is absorbed in γ.

Here, the kernel of the integral equation is separable in x and y. If the distribution function v is assumed to be of the form

$$v(x,y) = v_x(x) v_y(y) \tag{24}$$

it is possible to separate (23) into two equations, one involving x only and the other involving y only; that is,

$$v_x(x_2) = \gamma_x \int_{-a}^{a} K_x(x_2, x_1) v_x(x_1)\, dx_1, \tag{25a}$$

$$v_y(y_2) = \gamma_y \int_{-c}^{c} K_y(y_2, y_1) v_y(y_1)\, dy_1, \tag{25b}$$

with

$$K_x = \frac{e^{j(\pi/4)}}{\sqrt{\lambda b}} e^{-jk(x_1-x_2)^2/2b}, \tag{25c}$$

and

$$K_y = \frac{e^{j(\pi/4)}}{\sqrt{\lambda b}} e^{-jk(y_1-y_2)^2/2b}. \tag{25d}$$

The product of the eigenvalues γ_x and γ_y is equal to the eigenvalue γ in (23).

It remains to be shown that (25a) through (25d) represent integral equations for infinite strip mirrors. Let us consider a pair of infinite strip mirrors of width $2a$ and separated by b. The iterative equation for computing the field at the mirrors can be derived from (1). It is

$$u_{q+1}(x_2) = \frac{e^{j(\pi/4)}}{2\sqrt{\lambda}} \int_{-a}^{a} u_q(x_1) \frac{e^{-jk\rho}}{\sqrt{\rho}} \left(1 + \frac{b}{\rho}\right) dx_1, \tag{26}$$

where

$$\rho = \sqrt{b^2 + (x_1 - x_2)^2}.$$

For $(a^2/b\lambda) \ll (b/a)^2$, (26) reduces to

$$u_{q+1}(x_2) = \frac{e^{j[(\pi/4)-kb]}}{\sqrt{\lambda b}} \int_{-a}^{a} u_q(x_1)\, e^{-jk(x_1-x_2)^2/2b}\, dx_1. \tag{27}$$

The corresponding integral equation is

$$v(x_2) = \gamma \int_{-a}^{a} K(x_2, x_1)\, v(x_1)\, dx_1, \tag{28}$$

where

$$K(x_2, x_1) = \frac{e^{j(\pi/4)}}{\sqrt{\lambda b}}\, e^{-jk(x_1 - x_2)^2/2b} \tag{28a}$$

and the factor e^{-jkb} is absorbed in γ. We see that (25) and (28) are identical in form.

APPENDIX B

Circular Plane Mirrors

Assuming approximately plane waves propagating normally to the circular plane mirrors (Fig. 3), the iterative equation for computing the steady-state field distribution can be written as

$$u_{q+1}(r_2, \varphi_2) = \frac{j}{2\lambda} \int_0^a \int_0^{2\pi} u_q(r_1, \varphi_1)\, \frac{e^{-jkR}}{R} \left(1 + \frac{b}{R}\right) r_1\, d\varphi_1\, dr_1, \tag{29}$$

where

$$R = \sqrt{b^2 + r_1^2 + r_2^2 - 2r_1 r_2 \cos(\varphi_1 - \varphi_2)}.$$

If b/a is large, (29) simplifies to

$$u_{q+1}(r_2, \varphi_2) = \frac{je^{-jkb}}{\lambda b} \int_0^a \int_0^{2\pi} u_q(r_1, \varphi_1) \cdot e^{-jk[(r_1^2 + r_2^2)/2b - (r_1 r_2/b)\cos(\varphi_1 - \varphi_2)]} r_1\, d\varphi_1\, dr_1, \tag{30}$$

which is valid for $(a^2/b\lambda) \ll (b/a)^2$.*

The integral equation corresponding to (30) is

$$v(r_2, \varphi_2) = \gamma \int_0^a \int_0^{2\pi} K(r_2, \varphi_2; r_1, \varphi_1) v(r_1, \varphi_1) r_1\, d\varphi_1\, dr_1, \tag{31}$$

with

$$K(r_2, \varphi_2; r_1, \varphi_1) = \frac{j}{\lambda b}\, e^{-jk[(r_1^2 + r_2^2)/2b - (r_1 r_2/b)\cos(\varphi_1 - \varphi_2)]} \tag{31a}$$

---

* Comments in Appendix A regarding the stringency of this requirement are also applicable herein.

and where the factor e^{-jkb} is absorbed in γ. Making use of the relation[10]

$$e^{jn[(\pi/2)-\varphi_2]}J_n\left(k\frac{r_1r_2}{b}\right) = \frac{1}{2\pi}\int_0^{2\pi} e^{jk(r_1r_2/b)\cos(\varphi_1-\varphi_2)+jn\varphi_1}\,d\varphi_1 \qquad (32)$$

and integrating (31) with respect to φ_1, it is seen that

$$v(r,\varphi) = R_n(r)e^{-jn\varphi}, \qquad (n = \text{integer}) \qquad (33)$$

satisfies (31). The function $R_n(r)$ satisfies the reduced integral equation

$$R_n(r_2)\sqrt{r_2} = \gamma_n\int_0^a K_n(r_2, r_1)R_n(r_1)\sqrt{r_1}\,dr_1, \qquad (34)$$

with

$$K_n(r_2, r_1) = \frac{j^{n+1}k}{b}J_n\left(k\frac{r_1r_2}{b}\right)\sqrt{r_1r_2}\,e^{-jk(r_1^2+r_2^2)/2b}, \qquad (34a)$$

where J_n is a Bessel function of the first kind and nth order.

APPENDIX C

Confocal Spherical or Paraboloidal Mirrors

For confocal spherical mirrors of circular cross section (Fig. 4), the iterative equation corresponding to (29) is

$$u_{q+1}(r_2, \varphi_2) = \frac{j}{2\lambda}\int_0^a\int_0^{2\pi} u_q(r_1, \varphi_1)\frac{e^{-jkR}}{R}\left(1+\frac{b_1}{R}\right)r_1\,d\varphi_1\,dr_1 \qquad (35)$$

where

$$R = \sqrt{b_1^2 + r_1^2 + r_2^2 - 2r_1r_2\cos(\varphi_1 - \varphi_2)}.$$

The distance b_1 is given by

$$b_1 = b - \Delta_1 - \Delta_2 \qquad (36)$$

where, for confocal spherical mirrors,

$$\Delta_i = b - \sqrt{b^2 - r_i^2} \qquad i = 1,2. \qquad (36a)$$

If b/a is large, the distance Δ_i is given approximately by

$$\Delta_i \cong r_i^2/2b \qquad i = 1,2, \qquad (37)$$

which is exact for confocal paraboloids. In this case (35) simplifies to

$$u_{q+1}(r_2, \varphi_2) = \frac{je^{-jkb}}{\lambda b} \int_0^a \int_0^{2\pi} u_q(r_1, \varphi_1)\, e^{jk(r_1 r_2/b)\cos(\varphi_1 - \varphi_2)} r_1\, d\varphi_1\, dr_1, \quad (38)$$

which is valid for $(a^2/b\lambda) \ll (b/a)^2$.

The integral equation corresponding to (38) is

$$v(r_2, \varphi_2) = \gamma \int_0^a \int_0^{2\pi} K(r_2, \varphi_2; r_1, \varphi_1) v(r_1, \varphi_1) r_1\, d\varphi_1\, dr_1, \quad (39)$$

with

$$K(r_2, \varphi_2; r_1, \varphi_1) = \frac{j}{\lambda b} e^{jk(r_1 r_2/b)\cos(\varphi_1 - \varphi_2)} \quad (40)$$

and where the factor e^{-jkb} is absorbed in γ. Just as in the case of circular plane mirrors, it can be shown that

$$v(r,\varphi) = S_n(r) e^{-jn\varphi} \qquad (n = \text{integer}) \quad (41)$$

satisfies (39). The function $S_n(r)$ satisfies the reduced integral equation

$$S_n(r_2)\sqrt{r_2} = \gamma_n \int_0^a K_n(r_2, r_1) S_n(r_1) \sqrt{r_1}\, dr_1, \quad (42)$$

with

$$K_n(r_2, r_1) = \frac{j^{n+1}k}{b} J_n\left(k\frac{r_1 r_2}{b}\right)\sqrt{r_1 r_2}. \quad (42a)$$

REFERENCES

1. Schawlow, A. L. and Townes, C. H., Infrared and Optical Masers, Phys. Rev., **112,** 1958, p. 1940.
2. Maiman, T. H., Stimulated Optical Radiation in Ruby, Nature, **187,** 1960, p. 493.
3. Collins, R. J., Nelson, D. F., Schawlow, A. L., Bond, W., Garrett, C. G. B. and Kaiser, W., Coherence, Narrowing, Directionality and Relaxation Oscillations in the Light Emission from Ruby, Phys. Rev. Letters, **5,** 1960, p. 303.
4. Silver, S., *Microwave Antenna Theory and Design*, McGraw-Hill, New York, 1949, p. 167.
5. Hildebrand, F. B., *Methods of Applied Mathematics*, Prentice-Hall, Englewood Cliffs, N. J., 1952.
6. Connes, P., Increase of the Product of Luminosity and Resolving Power of Interferometers by Using a Path Difference Independent of the Angle of Incidence, Revue d'Optique, **35,** 1956, p. 37.
7. Lovitt, W. V., *Linear Integral Equations*, Dover Publications, New York, 1950, pp. 129; 137.
8. Goubau, G., and Schwering, F., On the Guided Propagation of Electromagnetic Wave Beams, URSI-IRE Spring Meeting, May 1960, Washington, D. C.
9. Boyd, G. D., and Gordon, J. P., Confocal Multimode Resonator for Millimeter through Optical Wavelength Masers, this issue, p. 489.
10. Stratton, J. A., *Electromagnetic Theory*, McGraw-Hill, New York, 1941, p. 372.